University of Wollongong
Research Online

Faculty of Science - Papers (Archive) | Faculty of Science, Medicine and Health

1-1-2011

Tectonic implications of early paleozoic metamorphism in the Anakie Inlier, central Queensland, Australia

R Offler
University of Newcastle

G Phillips

C L. Fergusson
University of Wollongong, cferguss@uow.edu.au

T J. Green

Follow this and additional works at: https://ro.uow.edu.au/scipapers

 Part of the Life Sciences Commons, Physical Sciences and Mathematics Commons, and the Social and Behavioral Sciences Commons

Recommended Citation

Offler, R; Phillips, G; Fergusson, C L.; and Green, T J.: Tectonic implications of early paleozoic metamorphism in the Anakie Inlier, central Queensland, Australia 2011, 467-485.
https://ro.uow.edu.au/scipapers/1094

Research Online is the open access institutional repository for the University of Wollongong. For further information contact the UOW Library: research-pubs@uow.edu.au

Tectonic implications of early paleozoic metamorphism in the Anakie Inlier, central Queensland, Australia

Abstract

Well-defined metamorphic zones are developed in pelitic and psammitic rocks of the Late Neoproterozoic to Cambrian Anakie Metamorphic Group of the Anakie Inlier, central Queensland. They are defined by the incoming of biotite, garnet, and andalusite, with or without staurolite. Mineral assemblages indicate that low pressure-high temperature metamorphism is associated with D1, medium pressure-high temperature metamorphism with D2, and retrograde, low pressure-low temperature metamorphism with D3. A mean b cell parameter of 9.035 obtained from K-white micas in the lowest-grade rocks suggests upper intermediate pressure conditions during D2. The timing of the growth of the index minerals indicates that isotherms retreated to the southwest during D2. Phase diagram calculations for both Al-saturated and Al-undersaturated metapelites containing D1 associations indicate pressure-temperature (P-T) conditions of 0.4 GPa and 560°C. These changed to 0.64-0.79 GPa and 580°-640°C as a result of crustal thickening. The samples thus record a history of heating (D1), followed by near-isothermal compression (D2). This P-T pathway shows that contraction rather than extension, as suggested by some authors, occurred during D2. The contractional event is suggested to have taken place during the Delamerian Orogeny as a result of convergence and collisional processes along the former passive margin of Gondwana.

© 2011 by The University of Chicago. All rights reserved.

Keywords

queensland, central, inlier, australia, anakie, tectonic, metamorphism, paleozoic, early, implications

Disciplines

Life Sciences | Physical Sciences and Mathematics | Social and Behavioral Sciences

Publication Details

Offler, R., Phillips, G., Fergusson, C. L. & Green, T. J. (2011). Tectonic implications of early paleozoic metamorphism in the Anakie Inlier, central Queensland, Australia. Journal of Geology, 119 (5), 467-485.

This journal article is available at Research Online: https://ro.uow.edu.au/scipapers/1094

Tectonic Implications of Early Paleozoic Metamorphism in the Anakie Inlier, Central Queensland, Australia

R. Offler,[1,] G. Phillips,[1] C. L. Fergusson,[2] and T. J. Green[2,†]*

1. Discipline of Earth Sciences, School of Environmental and Life Sciences, University of Newcastle, New South Wales 2308, Australia; 2. School of Earth and Environmental Sciences, University of Wollongong, New South Wales 2522, Australia

ABSTRACT

Well-defined metamorphic zones are developed in pelitic and psammitic rocks of the Late Neoproterozoic to Cambrian Anakie Metamorphic Group of the Anakie Inlier, central Queensland. They are defined by the incoming of biotite, garnet, and andalusite, with or without staurolite. Mineral assemblages indicate that low pressure–high temperature metamorphism is associated with D_1, medium pressure–high temperature metamorphism with D_2, and retrograde, low pressure–low temperature metamorphism with D_3. A mean *b* cell parameter of 9.035 obtained from K-white micas in the lowest-grade rocks suggests upper intermediate pressure conditions during D_2. The timing of the growth of the index minerals indicates that isotherms retreated to the southwest during D_2. Phase diagram calculations for both Al-saturated and Al-undersaturated metapelites containing D_1 associations indicate pressure-temperature (*P-T*) conditions of 0.4 GPa and 560°C. These changed to 0.64–0.79 GPa and 580°–640°C as a result of crustal thickening. The samples thus record a history of heating (D_1), followed by near-isothermal compression (D_2). This *P-T* pathway shows that contraction rather than extension, as suggested by some authors, occurred during D_2. The contractional event is suggested to have taken place during the Delamerian Orogeny as a result of convergence and collisional processes along the former passive margin of Gondwana.

Online enhancements: appendix tables.

Introduction

Metamorphic rocks in the Anakie Inlier of central Queensland represent a window of the widely spread yet buried rocks of the Thomson Orogen, eastern Australia (fig. 1; Withnall et al. 1995). They were derived from an assemblage of Neoproterozoic to Cambrian sedimentary and igneous units that formed along the passive margin of Gondwana (Fergusson et al. 2001, 2009). Significantly, these rocks record the transition from passive to convergent margin processes. The onset of convergent margin tectonism marks the initiation of the Tasmanide orogenic system and the manifestation of approximately 300 Ma of subduction-related orogenesis. Studying the rocks of the Anakie Inlier therefore provides insight into the kinematic and thermal evolution of a continental margin during a significant switch in tectonic setting.

A subhorizontal foliation (S_2) is a dominant feature of much of the Anakie Metamorphic Group and was thought to be related to a low-pressure metamorphic deformation event (Withnall et al. 1995). Whole-rock K-Ar ages that document cooling of the terrane are ca. 500 Ma. They have been used to suggest that the main deformation and metamorphism in the Anakie Inlier are related to the Ross-Delamerian Orogeny, which occurred in a convergent margin setting along the Panthalassan margin of Gondwana (Withnall et al. 1996; Cawood 2005). In the western part of the Anakie Inlier, the main regional foliation (S_2) dips steeply to the west, with metamorphic grade increasing upsection and culminating in the development of andalusite-garnet-staurolite schists. These features, along with

Manuscript received May 31, 2010; accepted May 25, 2011.

[1] Author for correspondence; e-mail: robin.offler@newcastle.edu.au.

[2] Present address: 8 Vitali Crescent, Kalgoorlie, Western Australia 6430, Australia.

[The Journal of Geology, 2011, volume 119, p. 467–485] © 2011 by The University of Chicago. All rights reserved. 0022-1376/2011/11905-0003$15.00. DOI: 10.1086/661191

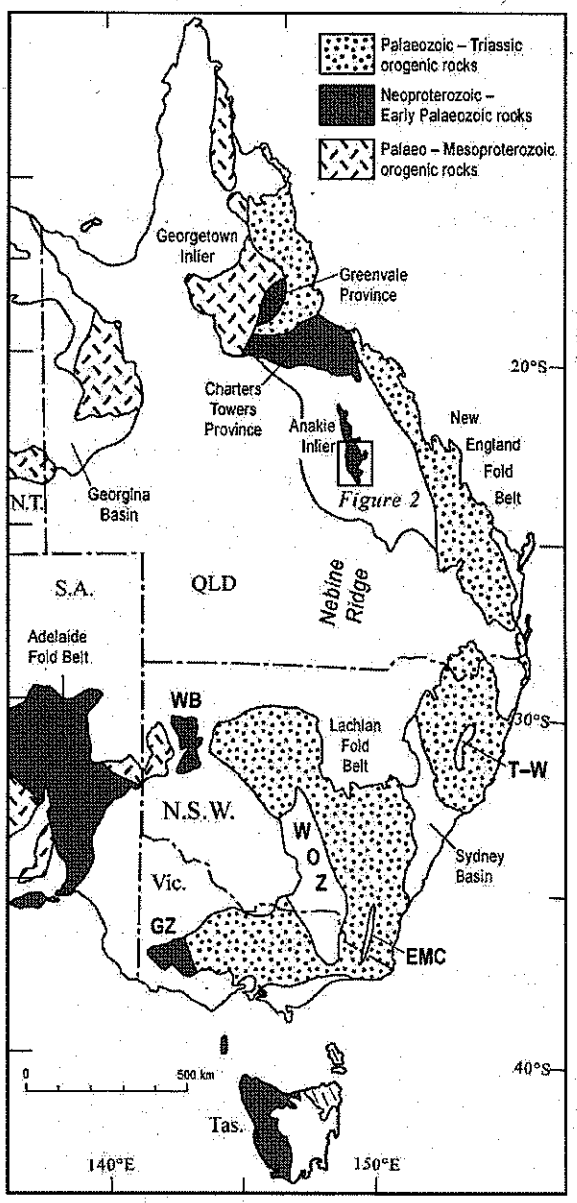

Figure 1. Location of the Anakie Inlier and the main orogenic rocks of eastern Australia. Low-pressure metamorphic rocks occur in the southeastern Adelaide Fold Belt, Glenelg Zone (*GZ*), and Wonominta Block (*WB*). *WOZ*, Wagga-Omeo Zone; *EMC*, eastern metamorphic complex; *T-W*, Tia-Wongwibinda (metamorphic complexes).

evidence for eastward-directed shear sense, were interpreted by Green et al. (1998) to be related to contractional deformation associated with ductile thrusting and uplift of deeper-level rocks in the west.

Low-angle, intense D_2 fabrics are widely developed in the metamorphic basement of the Charters Towers Province, ca. 400 km to the north (fig. 1), which has an age similar to that of the Anakie Metamorphic Group. These fabrics and associated metamorphism in the Cape River and Argentine metamorphics are thought to be related to a regional extension event that was also responsible for the formation of a backarc in the late Cambrian to Early Ordovician Seventy Mile Range Group (Fergusson et al. 2005, 2007). This event was dated at 490–460 Ma on the basis of $^{40}Ar/^{39}Ar$ and U-Pb zircon ages obtained from granitic rocks. By contrast, the age data in the Anakie Inlier indicate essentially 510–500-Ma deformation and metamorphism. This suggested to Fergusson et al. (2005, 2007) that the low-angle foliation in the inlier was formed in an earlier episode of extension during the Delamerian Orogeny and was unrelated to the Early Ordovician regional extension in the Charters Towers Province. By contrast, Wood and Lister (2004) proposed that extension took place during the formation of the Anakie Inlier as a metamorphic core complex.

These tectonic models are tested using new microstructural and metamorphic data presented here. Our aim is to document the metamorphic zonation and pressure-temperature (*P-T*) conditions of the Anakie Metamorphic Group in the region west of Clermont (fig. 2) where andalusite-staurolite-bearing schists occur. We also examine the relationships between deformation and metamorphism and from this determine the *P-T*-deformation paths in order to resolve the conflict between the roles of contraction and extension during the evolution of the Anakie Inlier. Evidence will be provided that shows that subhorizontal fabrics are not exclusively related to either core complex tectonics or extensional collapse. Pelitic rocks have been studied exclusively because they contain key metamorphic assemblages necessary for the determination of *P-T* conditions and relationships between deformation and metamorphism.

Anakie Metamorphic Group

The Anakie Inlier consists of the Late Neoproterozoic to Cambrian Anakie Metamorphic Group and less abundant Late Ordovician Fork Lagoons beds. The latter are in faulted contact with the Anakie Metamorphic Group and consist of arenites, cleaved mudstones, mafic lavas, and limestone lenses. The former are overlain unconformably by or are in faulted contact with Devonian limestone and silicic volcanic units similar to those at the

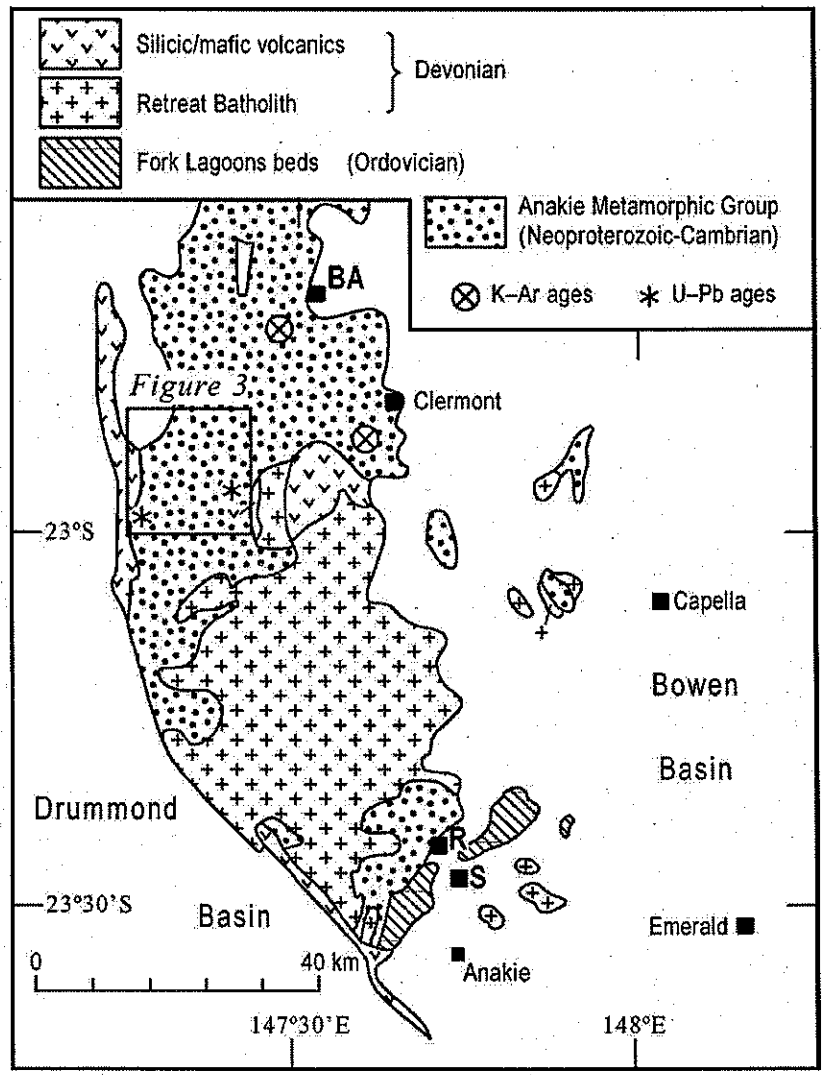

Figure 2. Map of the southern Anakie Inlier, with main pre-Carboniferous units shown (see fig. 1 for location). K-Ar age sites from Withnall et al. (1996). U-Pb age sites from Fergusson et al. (2001). *BA* = Blair Athol; *R* = Rubyvale; *S* = Sapphire.

base of the Devonian to Carboniferous Drummond Basin west of the inlier (fig. 2; Withnall et al. 1995). East of the inlier is the Permian to Triassic Bowen Basin. Basement units of the Anakie Inlier are considered part of the dominantly subsurface Thomson Fold Belt and, although buried, continue southward along the Nebine Ridge (Murray 1986; Withnall et al. 1995).

The Anakie Metamorphic Group has been subdivided into a number of units, four of which occur in the study area west of Clermont (fig. 3; Withnall et al. 1995). The Bathampton Metamorphics are structurally the lowest unit in the study area and contain pelitic and psammitic schists, quartzite, greenstone, and less abundant marble, calc-silicate rock, and serpentinite. They are overlain by the Rolfe Creek Schist, a unit dominated by pelitic schist with minor psammitic schists. This is in turn overlain by the Monteagle Quartzite, made up of quartzite and quartzose psammite, with less abundant graphitic and pelitic schists. The uppermost unit is the Wynyard Metamorphics, consisting of psammitic and less abundant pelitic schists. Detrital zircon ages indicate that quartz-rich psammite and metaconglomerate of the Bathampton Metamorphics are of probable Late Neoproterozoic

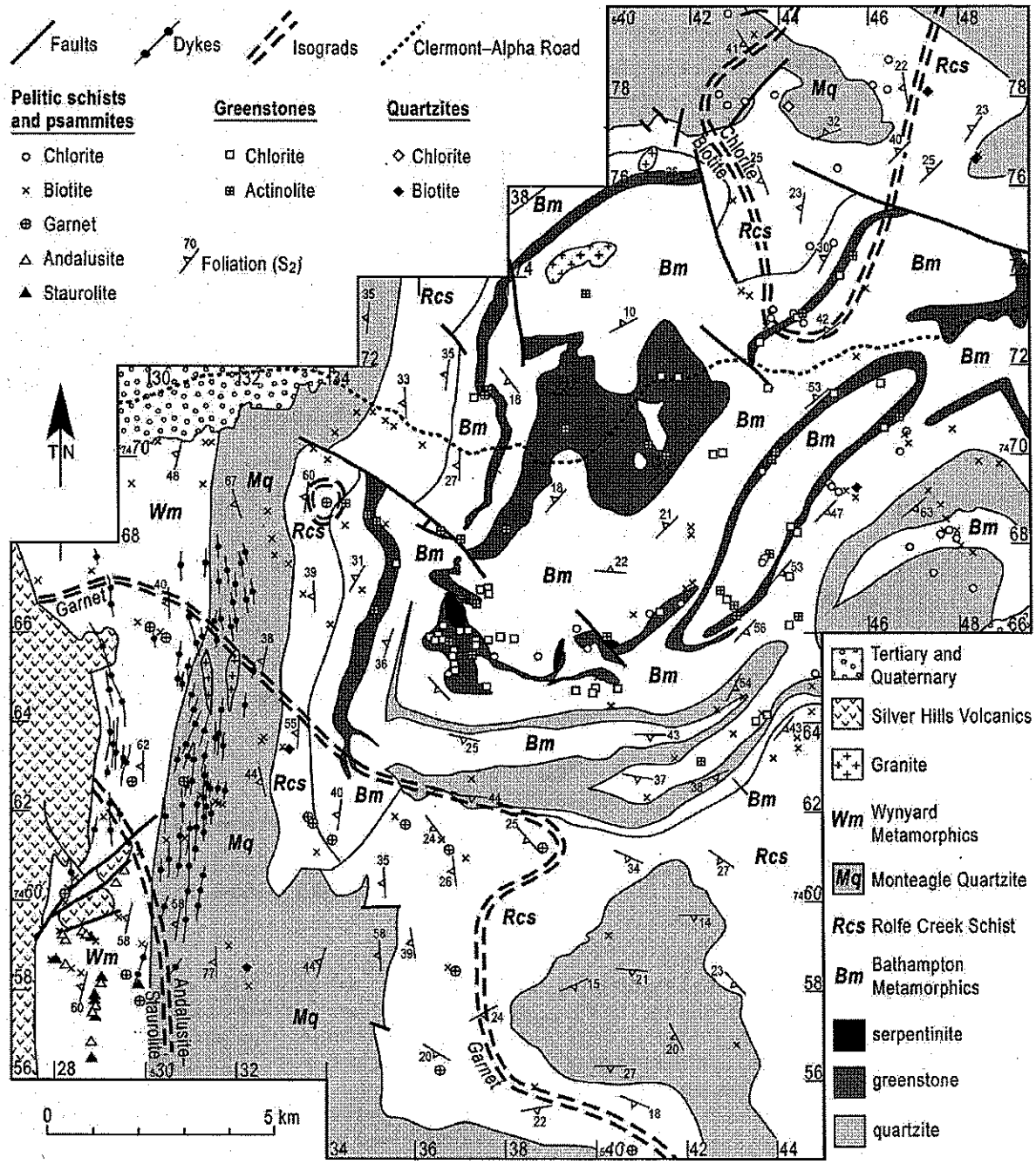

Figure 3. Map of the metamorphic zones in the Anakie Metamorphic Group to the west of Clermont, astride the Alpha-Clermont Road (see fig. 2 for location). The main lithological units are shown, along with larger greenstone and quartzite subunits of the Bathampton Metamorphics. Sample locations are shown for pelitic and psammitic schist, greenstone, and quartzite, with index metamorphic minerals. Contacts with the Silver Hills Volcanics and dikes in the western part of the area are after Davis and Henderson (1998) and Henderson et al. (1998).

age, whereas the Wynyard Metamorphics are of middle Cambrian age, consistent with their inferred stratigraphic order (Fergusson et al. 2001).

The structure and deformation history of the Anakie Metamorphic Group has been discussed by Withnall et al. (1995) and Green et al. (1998). Two main foliations are recognized, with the first (S_1) steeply dipping and defined by aligned micas and elongate quartz in pelitic and psammitic rocks. The second foliation (S_2) gently dips over much of the Anakie Metamorphic Group and is a crenulation cleavage with widespread mica growth in cleavage domains (Green et al. 1998). Abundant folds are associated with the second foliation, including map-scale near-recumbent folds. By contrast, macroscopic F_1 folds have been recognized in only two areas (Green et al. 1998). Strain fringes are widely developed around magnetite porphyroblasts and indicate that the D_2 deformation was associated with dominant vertical flattening, although late shear bands and asymmetric boudinage indicate some rotational component associated with this deformation (Green et al. 1998). Late-stage open folds associated with kinklike crenulation cleavages have affected the main S_2 foliation. In the western part of the Anakie Inlier, S_2 and associated structures have been tilted to steep to moderate angles to the west during deformation of the overlying Devonian Silver Hills Volcanics (fig. 3).

Timing of metamorphism and deformation in the Anakie Metamorphic Group is constrained by the inferred timing of deposition from detrital zircon ages obtained from the Wynyard Metamorphics near Eastern Creek (Fergusson et al. 2001) and the K-Ar ages of ~500 Ma, interpreted as cooling ages, from south of Clermont and near Blair Athol (fig. 2; Withnall et al. 1996). The youngest detrital zircon ages lie in the range 600–510 Ma (23 of 60 grains), indicating deposition in the interval 510–500 Ma (Middle Cambrian) if the K-Ar ages are assumed to have regional significance. Metamorphism and deformation therefore must have occurred in a relatively short interval after deposition in the middle Cambrian. Metamorphism predated deposition of the Lower Devonian Douglas Creek Limestone and intrusion of the Retreat Batholith in the Middle to Late Devonian (Withnall et al. 1995).

Techniques

Two and in some cases three sections of individual samples, including some cut parallel to the main foliation, were made in order to determine the timing of porphyroblast growth. We made note of size of inclusions in porphyroblasts relative to those in the matrix, as well as the orientation and curvature of inclusion trails. To determine the metamorphic conditions at which the assemblages from the low- to high-grade zones were formed, we applied several techniques, namely, x-ray diffraction (XRD) for the low-grade rocks (greenschist-subgreenschist facies), and energy-dispersive spectrometer (EDS) and mineral equilibria were used to calculate *P-T* for the higher-grade rocks.

X-Ray Diffraction. XRD analyses of K-white mica in 25 samples were carried out on a Philips automated PW1732/10 x-ray diffractometer, with CuKa radiation, graphite monochromator, and operating conditions of 40 kV/30 Ma.

Kübler Indices. Fractions of <2 μm were separated from whole-rock powders in distilled water, according to Stokes's law. To maintain a constant thickness, we pipetted approximately 3 mg cm^{-2} of sediment onto each slide. In this way, variation in intensity and peak width caused by changes in sediment thickness could be avoided (Kisch 1991; Krumm and Buggisch 1991). Samples were scanned over the range $2\theta = 6.5°–10°$ at 0.5° 2θ/min, using divergence slits of 1° and receiving slits of 0.1 mm. Illite crystallinity (Kübler 1968; now referred to as the Kübler Index [KI; Guggenheim et al. 2002]) was determined from the width of the (001) peak at half-peak height and expressed in terms of $\Delta 2\theta$ (Kisch 1991). KI values were then converted to Crystallinity Index Standard (CIS) values (Warr and Rice 1994), using calibration curves based on standards provided by L. N. Warr. These were then converted to Kübler-equivalent values by adding 0.04 to values obtained from the equation $KI_{Kisch\ equivalent} = 1.3056 \times KI_{Offler} - 0.1146$, based on CIS standards (see Kisch et al. 2004 for discussion).

Values indicate epizonal conditions if KI = 0.25 or less, anchizonal if 0.25 < KI < 0.42, and diagenetic if KI > 0.42. Table A1, available in the online edition or from the *Journal of Geology* office, summarizes the data obtained.

K-White Mica B *Cell Parameter.* To determine the *b* cell dimensions of K-white micas, we obtained diffractograms from <2-μm powders packed into aluminium mounts, similar in design to that of Robinson (1981), to enhance the (060) peak relative to the (3̄31) peak (Guidotti 1984). The range $2\theta = 59.5°–63°$ was step scanned at 0.005° 2θ/s, using a counting time of 1 s, and the *b* cell dimension was determined from the (060) peak, using the (211) quartz reflection as an internal standard. Machine settings were slits 2°, 0.1 mm, 2°, and time constant 2.

Determination of this parameter is normally per-

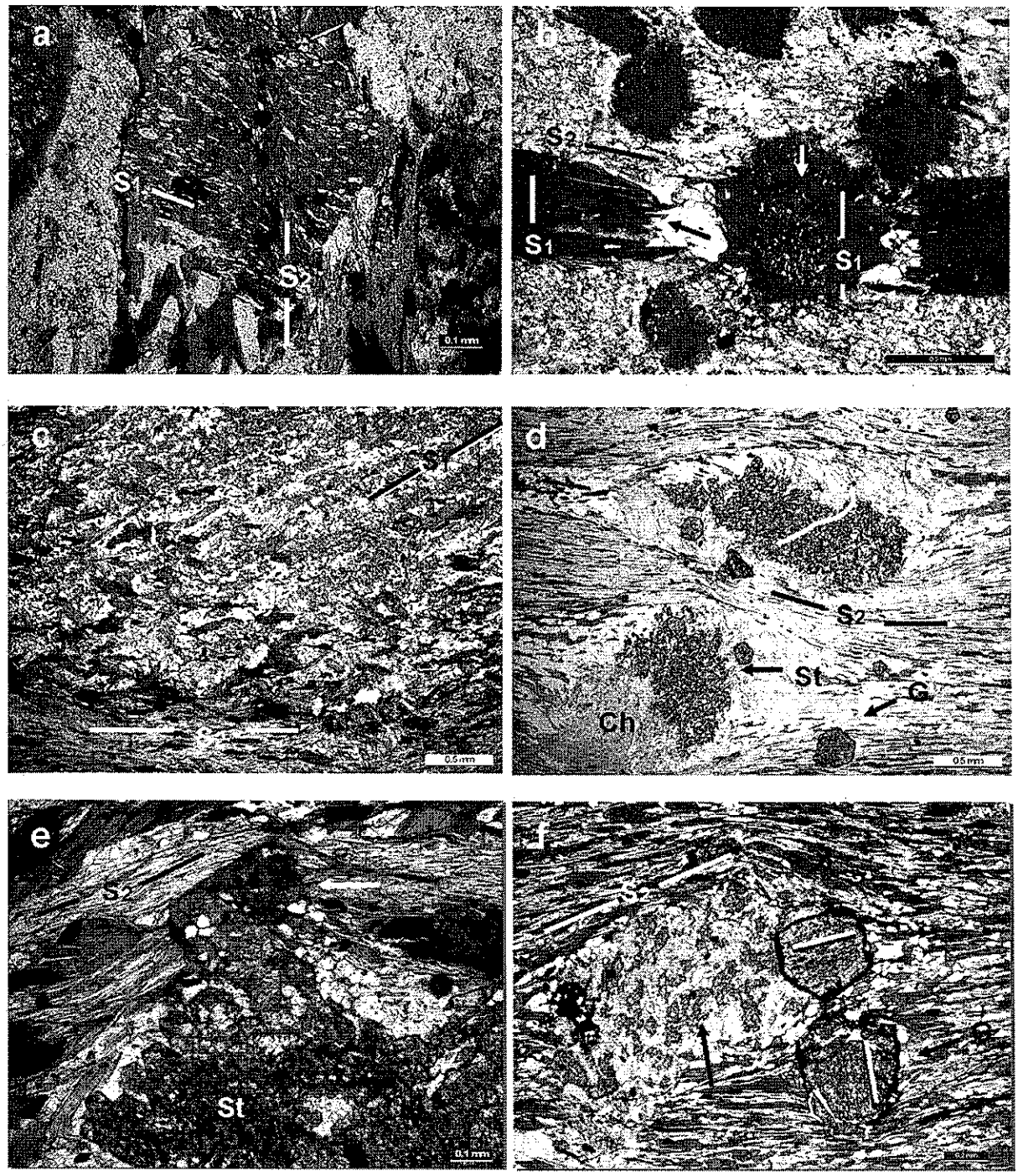

Figure 4. *a*, Post-D_2 biotite porphyroblast, showing inclusion trails defining crenulated S_1 and N-S trending S_2. Biotite zone. Sample A210. *b*, Photomicrograph showing post-D_1 and syn-D_2 biotite growth (*black arrow*). *White arrow* = inclusion trails of quartz-defining S_1 in biotite. Garnet zone. Sample A353. *c*, S_2 defined by muscovite and biotite flattened against pre-D_2 andalusite. Andalusite-staurolite zone. Sample A335. *d*, Early syn-D_2 staurolite (*St*) containing curved inclusion trails defined by quartz (*white line*) and post-D_1 garnet (*G, arrow*). Late post-D_2 chlorite (*Ch*) also

formed on slates or phyllites that record only one deformation event. In this study, multiply deformed samples have been analyzed; thus, interpretation of data requires careful petrographic examination of individual samples to ascertain which white micas are responsible for the values obtained. Data obtained from the samples are shown in table A1.

Energy-Dispersive Spectrometer. Mineral compositions were determined on a Philips XL30 scanning electron microscope with attached IS200 EDS at the University of Newcastle. Operating conditions involved a counting time of 60 s and accelerating voltage of 15 kV and 0.2 nA. Data were collected as weight percent oxides, and stoichiometric formulas were determined using standard techniques outlined by Deer et al. (1992). Mica, chlorite, and garnet analyses were normalized to 22, 28, and 12 oxygens, respectively. Fe^{3+} was calculated according to the method of Droop (1987). Special care was taken in choosing garnets that were unaltered and not in contact with biotite, with which Fe-Mg exchange could take place.

X-Ray Fluorescence. Major elements were determined by standard XRF methods at the University of Newcastle, using a Spectro X-Lab 2000. All analyses were performed on fused discs made from rock powders produced by grinding rock chips in a Tema WC mill. Analyses are listed in table A2, available in the online edition or from the *Journal of Geology* office.

Metamorphic Zones

Examination of more than 350 thin sections of pelitic and psammopelitic rocks revealed four metamorphic zones (in order of increasing grade: chlorite, biotite, garnet, and andalusite-staurolite; fig. 3). The incoming of particular index minerals (e.g., garnet), as will be shown for samples in the andalusite-staurolite zone, is very much dependent on the bulk composition of the host rock.

Chlorite Zone. The lowest-grade rocks are limited to the northeast of the study area and comprise quartz + muscovite ± chlorite ± albite ± ilmenite ± magnetite. Opaque minerals generally make up less than 1% of the rock. Samples record evidence for two and in some cases three or more deformation events (D_1, D_2, D_3, and D_4). Samples affected by D_2 show a well-developed crenulation cleavage (S_2) made up of closely packed muscovite ± chlorite ± carbonaceous aggregates ± ilmenite. In lower-strain samples, crenulated S_1 is defined by muscovite showing intracrystalline strain and less common ilmenite in P domains and by quartz, muscovite, and chlorite in Q domains in lower-strain samples. Quartz veins forming isoclinal fold hooks (F_2) and pinch-and-swell structures parallel to S_2 are present in some samples. Quartz commonly exhibits a static recrystallization texture and, when affected by D_3, moderate to strong undulose extinction, grain boundary migration, and healed fractures. Post-D_2 tourmaline forms in some samples, as do syn-D_2 strain fringes containing quartz ± chlorite ± biotite, adjacent to magnetite and pyrite porphyroblasts. D_3 is manifested by crenulations, open to tight folds defined by S_2, and uncommon crenulation cleavage (S_3), which is a solution cleavage.

Metapelites from both the Bathampton Metamorphics and the Rolfe Creek Schist occur within this zone; however, no discernible variation occurs in metamorphic assemblage between the two tectonostratigraphic units. Quartzite of the Monteagle Quartzite is represented in the chlorite zone and comprises quartz + albite ± muscovite ($Na_{0.06-0.09}$) ± chlorite.

Biotite Zone. In the biotite zone (fig. 3), metapelitic rocks of both the Bathampton Metamorphics and the Rolfe Creek Schist have the assemblage quartz + muscovite ($Na_{0.03-0.14}$) + biotite ± chlorite ± albite ($An_{0.2-1.9}$) ± magnetite ± ilmenite ± graphite; tourmaline is an accessory mineral. The boundary between the chlorite and biotite zones is in places difficult to resolve because of replacement of biotite by chlorite during the D_3 event. Most chlorite in this zone is secondary after biotite; however, some "armored" grains of chlorite exist within recrystallized quartz. These rocks display a well-developed crenulation cleavage (S_2) defined by a solution cleavage in the lower-grade northeast part of the biotite zone and by biotite, smaller muscovite laths, and ilmenite to the southwest. Between the mica-rich S_2 domains are quartz-rich domains containing S_1 defined by muscovite and biotite oblique to S_2. In many rocks, biotite occurs as post-D_1, early syn-D_2, and late syn-D_2 porphyroblasts with either straight or sigmoidal inter-

present. Andalusite-staurolite zone. Sample A344. *e*, Syn-D_2 staurolite. White arrow points to late syn-D_2 growth that has been altered to fine-grained retrograde white mica. Andalusite-staurolite zone. Sample A335. *f*, Relict pre-D_2 staurolite (*arrow*) replaced by fine-grained retrograde white mica and garnet (*G*). White bars in garnet outline S_1. Note difference in orientation of S_1 in garnet. Andalusite-staurolite zone. Sample A340B.

nal inclusion trail S_i that is often continuous with external foliation S_e (fig. 4*a*). S_i in the porphyroblasts is defined by quartz ± albite, oblique to S_2. Strain fringes containing quartz ± chlorite ± biotite are common adjacent to magnetite crystals. Post-D_1 biotite porphyroblasts are common. Biotite blades may be attached to them and aligned parallel to S_2, indicating that growth has occurred continuously from post-D_1 to syn-D_2. Near the garnet zone, biotite locally defines a stretching lineation. Psammitic rocks and quartzite have similar assemblages but show more quartz and albite. In both the chlorite and biotite zones, randomly distributed magnetite porphyroblasts (0.2–1 mm across) occur and show well-developed strain fringes made up of recrystallized quartz ± chlorite ± micas. In the central and eastern part of the study area, a folded D_2 biotite zone boundary can be delineated.

Garnet Zone. The garnet zone occurs in the western part of the study area, and the boundary with the biotite zone is curved as a result of folding during the D_3 event. In contrast to the pelitic rocks within the Rolfe Creek Schist, those in the other units consist of quartzite and psammitic rocks. Metapelitic rocks have the assemblage quartz + muscovite ($Na_{0.23–0.4}$) + biotite ± chlorite (generally secondary) + garnet ± plagioclase ($An_{18–29}$) ± magnetite ± ilmenite ± graphite; tourmaline is an accessory mineral. Garnet porphyroblasts are typically 0.25–1 mm across. S_i-S_e relationships indicate that the garnet grew post-D_1–early syn-D_2 or post-D_2. It first appears post-D_1–pre-D_2 in the northwest part of the area and post-D_2 in the southeast. Biotite porphyroblasts have a similar growth history, showing evidence for both post-D_1 and early syn-D_2 crystallization. S_2 is a crenulation cleavage defined by biotite and muscovite that wrap around these porphyroblasts and across which post-D_2 chlorite and ilmenite have grown. In the psammitic samples, post-D_1 biotite porphyroblasts are common. Biotite blades may be attached to them and aligned parallel to S_2, indicating that growth has occurred continuously from the intertectonic period to the syntectonic period (fig. 4*b*).

Andalusite-Staurolite Zone. The highest-grade rocks in the study area occur in the southwestern part of the area around Eastern Creek (andalusite-staurolite zone; fig. 3) and include rocks with four or more of the following: andalusite, staurolite, biotite, muscovite ($Na_{0.28–0.58}$), quartz, plagioclase, and garnet (fig. 5). Variation in mineral assemblage is controlled by bulk chemistry and by changes in *P* that have occurred during crustal thickening. Originally, separate andalusite and staurolite zones were mapped (Fergusson et al. 2001; fig. 3), but more detailed work has shown that these two zones are overlapping (fig. 3). Most of the andalusite porphyroblasts have rectangular outlines and are replaced by prograde coarse muscovite and retrograde, fine-grained white mica. They are 1–10 mm in length, and their Si contents suggest that they have grown intertectonically post-D_1 (fig. 4*c*). Chiastolite is uncommon and observed as altered porphyroblasts showing cruciform patterns of carbonaceous inclusions (e.g., TS11710, A339). Other inclusions have a random orientation in sections of different orientation, suggesting growth pre-D_1. However, it is unclear whether the inclusions are inherited or are a by-product of the replacement of the andalusite and other phases in this sample by retrograde white mica. Staurolite may grow separately or together with andalusite. It is 1–2 mm across and is generally preserved as post-D_1 and early syn-D_2 porphyroblasts partially to completely altered to fine-grained white mica (fig. 4*d*, 4*e*). Minor post-D_2 growth has also been noted (e.g., A335). Garnet records similar stages of growth and in some samples has formed post-D_2 (fig. 5). Biotite either forms post-D_1–pre-D_2 intertectonic porphyroblasts or defines S_1 and S_2. Biotite, andalusite, staurolite, and garnet porphyroblasts have strain fringes that are symmetrical and elongate parallel to S_2. Chlorite may replace garnet or form post-D_2 chlorite porphyroblasts.

Metabasic Rocks

Greenstones within the study area are contained almost entirely within the chlorite and biotite zones. They do not show any apparent systematic change in assemblage across the biotite isograd and contain rocks with relatively few mineral phases compared with the metapelites. Thus, fewer metamorphic zones can be delineated. Most samples examined contain chlorite ± quartz ± calcite ± albite. Epidote is common in many samples, and clinozoisite is present in some samples. Actinolite is less common in the greenstones within the study area, and when present, it commonly occurs as post-D_2 decussate crystals. Magnetite is common in samples from the two metamorphic zones and often exhibits fringes containing chlorite ± recrystallized quartz ± (calcite). Ilmenite is an additional phase.

Relationship between Metamorphism and Deformation

Two main foliations, S_1 and S_2, are evident throughout the study area; the degree of mineral alignment

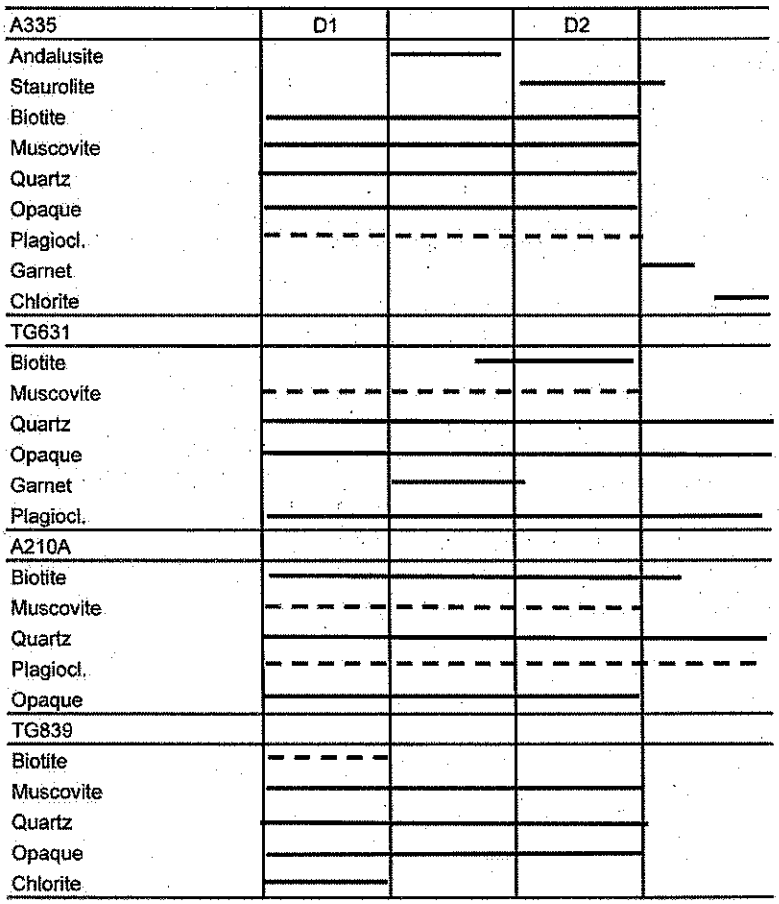

Figure 5. Chronology of mineral growth in samples from metamorphic zones.

associated with each varies. In the chlorite and biotite zones, S_1 is defined by aligned muscovite ± chlorite ± biotite, indicating that greenschist facies metamorphism was synchronous with D_1 (fig. 5). S_2 is a well-developed crenulation cleavage, and in many samples, neocrystalline white micas define S_2, indicating greenschist facies conditions during D_2. However, not all samples show this, and in some, especially in the chlorite zone, S_2 is defined by closely packed white mica ± ilmenite, formed by the dissolution of the limbs of tight to isoclinal folds in S_1. In these samples, it is difficult to ascertain whether the white mica is neocrystalline or the result of reorientation of S_1. Samples in the northeast part of the area commonly show biotite parallel to S_1 and S_2 by closely spaced white mica. Crenulated white mica and quartz in domains between S_2 are strongly deformed and not recrystallized, suggesting that *T* had fallen during D_2.

In some samples, strain fringes elongate parallel to S_2 are well developed around magnetite porphyroblasts and are composed of mainly quartz. Some include micas and/or chlorite, consistent with greenschist metamorphic conditions during D_2. Post-D_2 growth of biotite is evident in some samples (fig. 4*a*). Kinking in the micas and well-developed undulose extinction observed in quartz are found in rocks showing D_3 fabrics. In summary, peak metamorphism predated, accompanied, and postdated D_2 in all but the northeast part of the area.

At higher metamorphic grades, S_1 is less evident and S_2 is associated with abundant aligned biotite and muscovite. Garnets in samples from the garnet zone grow either early post-D_1 or post-D_2 (fig. 5). Biotite, andalusite, staurolite, and garnet porphyroblasts have associated with them symmetrical strain fringes that are elongate parallel to the S_2 foliation, indicating that they developed during D_2. Inclusion trails in these porphyroblasts are straight and oblique to S_2 in some samples and thus have formed intertectonically (fig. 4*b*, 4*c*); in others, the

inclusion trails have a sigmoidal outline so that the internal inclusion trail is curved into micas defining S_2 at the margin of the porphyroblast, indicating early syn-D_2 growth (fig. 4*d*). Syntectonic growth is also indicated by S_2 flattened against porphyroblasts containing rims with inclusion trails parallel to and continuous with S_2. In some samples, varying orientations of inclusion trails occur in garnet porphyroblasts, suggesting that they grew in former crenulation hinges or were rotated during deformation of the matrix (Vernon et al. 1993). The occurrence of garnets in domains with parallel inclusion trails supports the first interpretation. Other samples show several stages of growth of porphyroblasts. These are recorded in biotite (post-D_1, syn-D_2; fig. 4*b*) and staurolite (syn-D_2, post-D_2, e.g., A335; fig. 4*e*). Such observations indicate that the higher-grade metamorphism predated and continued after D_2. In the garnet and andalusite-staurolite zones, post-D_2 chlorite porphyroblasts are widely developed, showing that temperature decreased post-D_2. In rare cases, late biotite porphyroblasts are also developed. These late porphyroblasts are invariably internally kinked, showing that D_3 postdated their development.

Results

Kübler Indices and b Cell Parameters. KI values range from 0.24 to 0.42 (table A1), indicating epizonal to anchizonal (greenschist to prehnite pumpellyite facies) conditions. The *b* cell parameters range from 9.008 to 9.050 and have a mean value of 9.035 ($n = 25$, $\sigma n = 0.011$). A few samples record low *b* cell parameter values (table A1).

Mineral Chemistry. *Garnet.* EDS analyses and x-ray maps of individual garnet grains reveal that they are almandine rich and grossular and pyrope poor (table A3, available in the online edition or from the *Journal of Geology* office). Post-D_2 garnet in sample A335 from the andalusite-staurolite zone shows little variation in composition from core to rim (fig. 6; $X_{Alm} = 0.66–0.68$, $X_{Sps} = 0.18–0.20$, $X_{Grs} = 0.05–0.07$, $X_{Prp} = 0.70–0.88$, $X_{Fe} = 0.88–0.90$; table A3). There appears to be no evidence for diffusion subsequent to growth. By contrast, post-D_1 garnet in sample TG631 reveals an increase in X_{Alm} from core to rim (0.547–0.742) and a decrease in X_{Sps} (0.29–0.126), resulting in a bell-shaped profile (figs. 6, 7). Pyrope and grossular contents remain constant and similar to garnets in the highest-grade zone. These features indicate that there was little change in *T* during their growth.

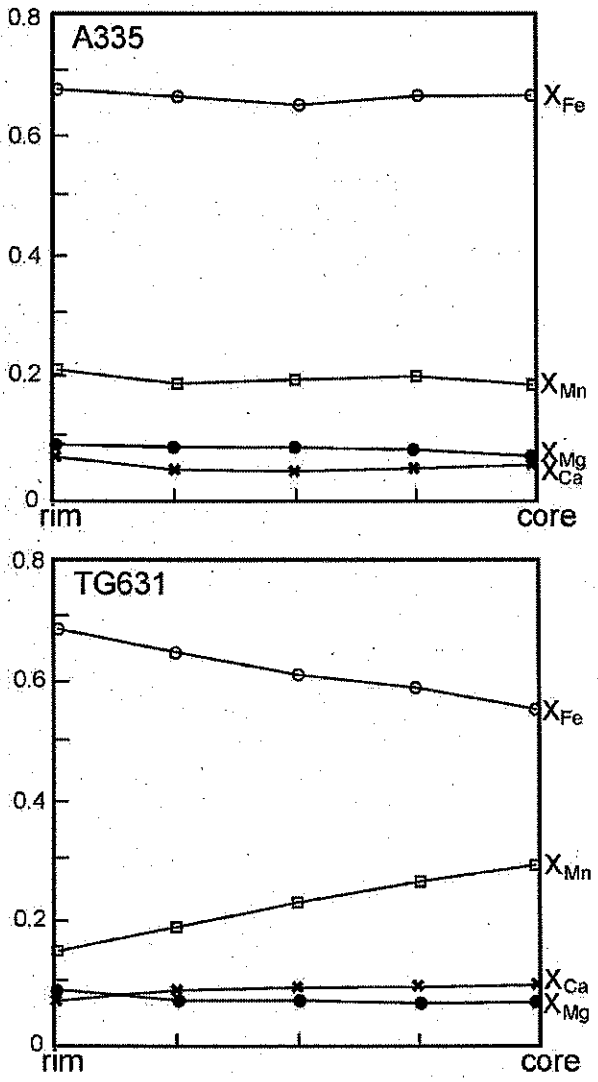

Figure 6. Garnet compositional plots of A335 (andalusite-staurolite zone) and TG631 (garnet zone).

Biotite. Biotites analyzed occur in ilmenite-bearing assemblages containing aluminous minerals. Thus, Al, Si, and Ti are at near-saturation levels, and the affect of bulk composition on their composition at a given temperature is limited (Henry et al. 2005). They are peraluminous and show minor changes in composition with increase in grade, namely, a decrease in Ti and an increase in $Al^{iv} + Al^{vi}$ (fig. 8; table A4, available in the online edition or from the *Journal of Geology* office). This trend is due to the $TiRAl_{-2}$ and Al_2R_{-3} exchange vectors, where *R* represents the sum of divalent cations in the octahedral sites (Henry et al. 2005). Such exchange vectors are confirmed in other plots

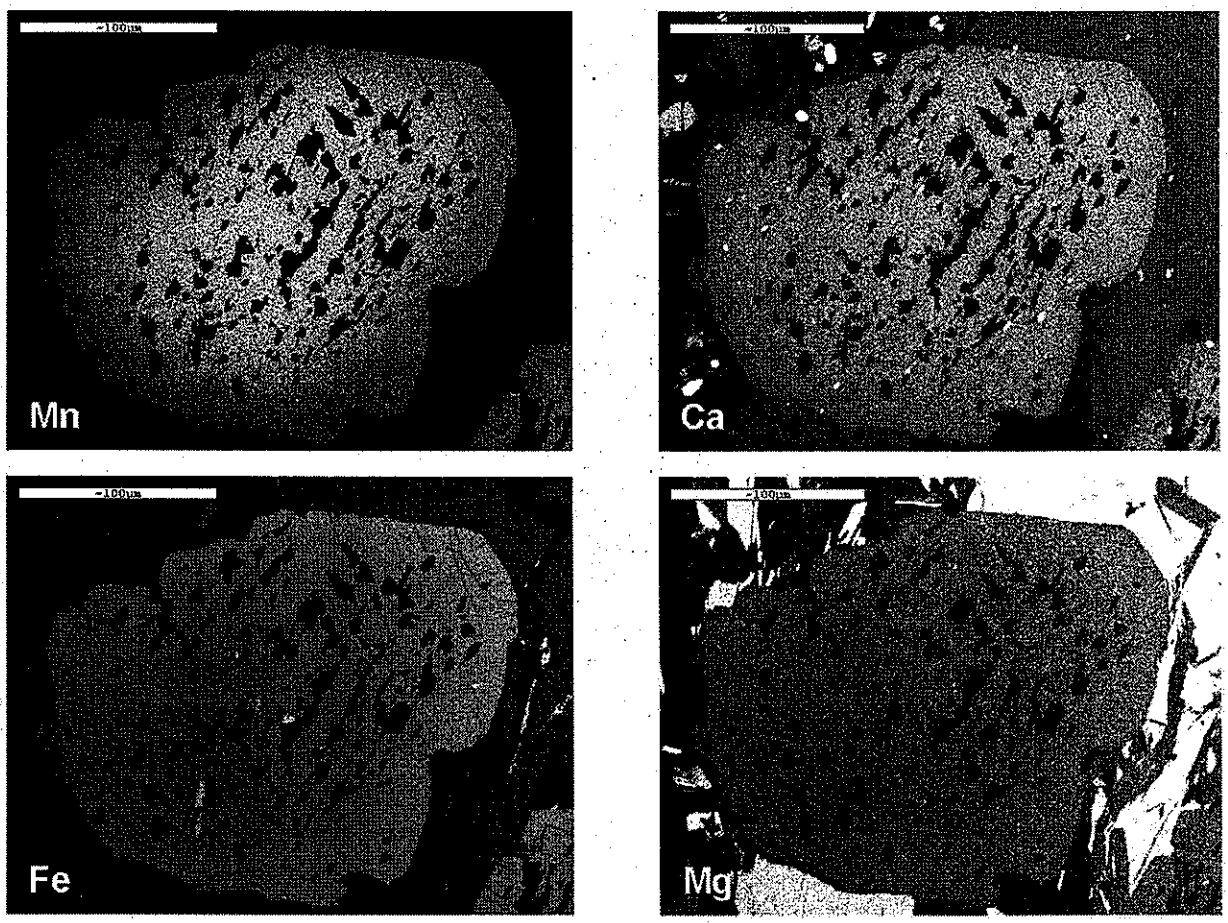

Figure 7. X-ray maps of garnet porphyroblast in sample TG631. Note decrease in Mn content from core to rim.

involving biotites from individual zones (e.g., $2Al^{vi}$ vs. $3(Mg + Fe^{2+} + Mn)$; Ti vs. $(Mg + Fe^{2+} + Mn)$). Biotite grains from samples of the same grade and that have formed post-D_1 and syn-D_2 have similar Ti contents.

Muscovite. In rocks from the chlorite and biotite zone in which biotite occurs as a minor pre-D_2 phase, white micas defining S_1 and S_2 are moderately Si and Fe + Mg rich (table A4; fig. 9). Si contents of S_2 muscovite vary more than those defining S_1. Average Si contents for muscovites are S_1 = 6.390 (n = 4), S_2 = 6.365 (n = 2; TG839), S_1 = 6.354–6.410 (n = 7), and S_2 = 6.464–6.533 (n = 9; A251, A744). With increasing grade, Si decreases (fig. 9), and paragonite ($Na_{0.30-0.36}$) increases. The former is related to the tschermak exchange vector between muscovite and celadonite ($Al_2Mg_{-1}Si_{-1}$), the latter to replacement of K by Na with increasing temperature (Parra et al. 2002). Si contents (6.06–6.14) of the highest-grade muscovites are similar to those recorded in high-grade rocks from other metamorphic terrains and calculated thermodynamically (Guidotti 1984; Zhu and Wei 2007).

Post-D_2 muscovite porphyroblasts in andalusite-staurolite schist have compositions similar to muscovite-defining S_2, indicating that they have formed under similar high T–moderate P metamorphic conditions. Retrograde, fine-grained white mica, on the other hand, is generally richer in (Fe+Mg) and Si than its high-grade counterparts, reflecting lower P-T conditions of formation.

Chlorite. Compositionally, the post-D_2 chlorites found in all samples are type 1 Mg- or Fe-chlorites (Zane and Weiss 1998; table A4). Tetrahedral Al contents suggest approximate temperatures of formation of 380°–398°C for posttectonic

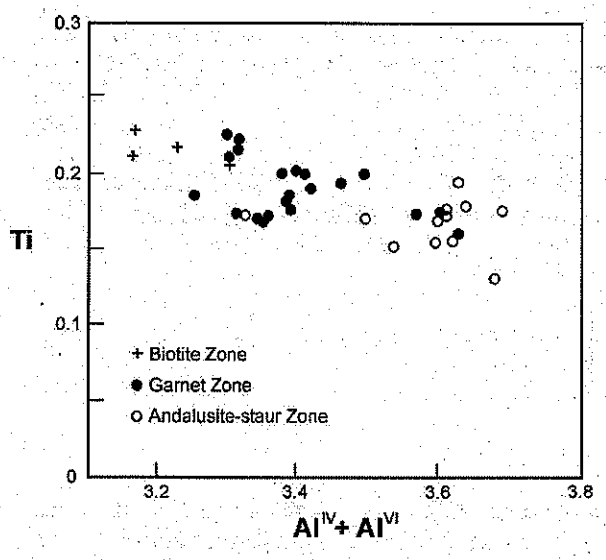

Figure 8. Compositional variation of biotites-Ti-$Al^{iv}+Al^{vi}$ plot.

chlorites in samples from the andalusite-staurolite zone and 331°–357°C for those in the biotite zone, according to the regression equation of Hillier and Velde (1991). The chlorites in these samples are uncontaminated by other fine-grained intergrown minerals and do not contain mixed layers, as do those in very low-grade rocks; therefore, the temperatures obtained are probably reliable, despite the criticisms leveled at the chlorite geothermometer by Jiang et al. (1994).

Discussion

Kübler Indices and b Cell Parameters. The samples show a wide range in KI values, and many record much higher values than normally determined from rocks subjected to greenschist facies conditions. This increase in KI may be related to crystallite size because it has been shown by Árkai et al. (1997) in their studies of samples from the Glarus overthrust that crystallite size decreases and KI increases as the thrust is approached. They attributed the decrease in crystallite size to increasing shear strain. The higher values obtained in this study may be related, therefore, to decrease in crystallite size produced in S_2 micas during D_3, affecting samples to varying degrees.

The samples record a mean *b* dimension value of 9.035, indicating upper intermediate-*P* conditions (Guidotti and Sassi 1986). However, pelites from the chlorite zone show evidence for two or more deformation events, the most prominent of which is D_2. This would imply that the *b* dimensions reflect *P-T* conditions operating during D_2, an interpretation acceptable for many of the samples that are dominated by S_2. However, in samples containing both S_1 and S_2, some contribution from S_1 might be expected, and evidence for this appears in XRD patterns. This was not observed; thus, it must be assumed that the *b* values reflect the metamorphic conditions prevailing during D_2.

A few samples contain very minor quantities of post-D_1–pre-D_2 biotite. Normally, when this mineral is present, Fe and Mg partition into biotite, lowering the celadonite content of the coexisting white mica and consequently the *b* cell parameter value. This does not appear to have happened in the samples analyzed. The reason for this is revealed in the studies of Sillanpää (1986), who showed that with the first appearance of biotite, celadonite content is only slightly lowered in white mica. This observation suggests that the small difference in *b* dimensions of biotite-absent and biotite-present samples in the study area is because biotite is present in small quantities. Thus, the data obtained from white micas in biotite-bearing samples truly reflect metamorphic conditions. Assuming a temperature of approximately 350°C for the lower greenschist facies assemblages observed in the low-grade samples from which the data were obtained, we calculate *P* of approximately 0.55 GPa during D_2 from the *P-T-b* space plot of Guidotti and Sassi (1986).

Phase Equilibria. Metamorphism within the study area is of low to medium grade. At the highest grade, the widespread development of andalusite, garnet, and staurolite provides a limit on pressures

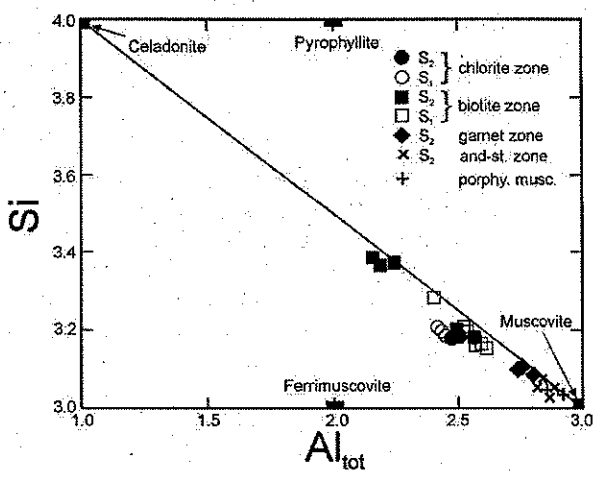

Figure 9. Si-Al_{tot} plot for muscovites from various zones.

operating during the deformation events. Additional information on conditions of metamorphism comes from the composition of garnets and biotites in the higher-grade rocks (A335, TG631). Garnets show little variation in X_{Fe}, X_{Grs}, X_{Prp}, and X_{Sps} from core to rim, suggesting that changes in T and P during growth were small (table A3). Limited variation in Ti contents of biotites formed during D_1 and D_2 also occur, indicating that near-isothermal conditions prevailed during crustal thickening associated with deformation. Temperatures based on the Ti contents and X_{Mg} of biotite from the highest-grade assemblages (Henry et al. 2005) vary from 536°C during D_1 to 541°–544°C during D_2 (table 1).

To constrain P-T conditions and determine a P-T path for the rocks in the study area, we constructed pseudosections for low (A335) and high (A339) Al metapelites from the Wynyard Metamorphics that contained critical assemblages (figs. 5, 10). Thermocalc 3.5 (Powell and Holland 1988) and the internally consistent data set of Holland and Powell (1998) were used for phase diagram calculations. Calculations for these samples were undertaken in the chemical system MnO-Na_2O-CaO-K_2O-FeO-MgO-Al_2O_3-SiO_2-H_2O-TiO_2-Fe_2O_3 (MnNCKFMASHTO), applying the following a-x relationships: garnet, biotite, and ilmenite (White et al. 2005); chlorite (Mahar et al. 1997); muscovite/paragonite (Coggon and Holland 2002); staurolite (Mahar et al. 1997); plagioclase (Holland and Powell 2003); epidote (Holland and Powell 1998); and magnetite (White et al. 2000).

Phase Diagram. *Sample A335.* The phase diagram shown in figure 10*a* illustrates phase relations in a low-Al metapelite (table A2). The D_1 mineral assemblage in sample A335 is characterized by andalusite, staurolite, biotite, muscovite, plagioclase, and ilmenite, with excess quartz. Phase diagram calculations indicate that this multivariant assemblage is stable over a small area of P-T space, namely, 0.42–0.4 GPa and 570°–560°C (fig. 10*a*). D_2 reaction microstructures are characterized by the

Table 1. Temperature and Pressure Determined from Various Geo- and Thermobarometers and Pseudosections

Sample	Assemblage	Average Al_{iv} chlorite	Average Ti biotite	n	Temperature (°C)[a]	Pressure (GPa)	Zone
TG839	Quartz-chlorite-muscovite	2.64 (syn-D_1)	...	2	333	...	Chlorite
TG744	Quartz-chlorite-muscovite-albite-(biotite-pre-D_2)	2.69 (syn-D_1)	...	3	345	...	Biotite
A251	Quartz-chlorite-muscovite-biotite	2.74 (syn-D_1, D_2)	...	3	358	...	Biotite
A335	Quartz-muscovite-biotite-garnet-staurolite-andalusite-plagioclase	2.89 (post-D_2)	...	1	397	...	Andalusite-staurolite
A335	Quartz-muscovite-biotite-garnet-staurolite-andalusite-plagioclase	...	.167 (S_2)	3	542	...	Andalusite-staurolite
A335	Quartz-muscovite-biotite-garnet-staurolite-andalusite-plagioclase	...	.185 (S_1)	2	563	...	Andalusite-staurolite
A335	Quartz-muscovite-biotite-garnet-staurolite-andalusite-plagioclase	D_1	...	...	560[b]	.4[b]	Andalusite-staurolite
A335	Quartz-muscovite-biotite-garnet-staurolite-andalusite-plagioclase	D_2	...	...	600[b]	.64–.79[b]	Andalusite-staurolite
EC03	Quartz-muscovite-biotite-staurolite-chlorite	2.79 (post-D_2)	...	3	388	...	Andalusite-staurolite
EC03	Quartz-muscovite-biotite-staurolite-chlorite	...	.169 (S_2)	4	551	...	Andalusite-staurolite

[a] Temperature determined from Henry et al. (2005).
[b] Temperature and pressure determined from pseudosection.

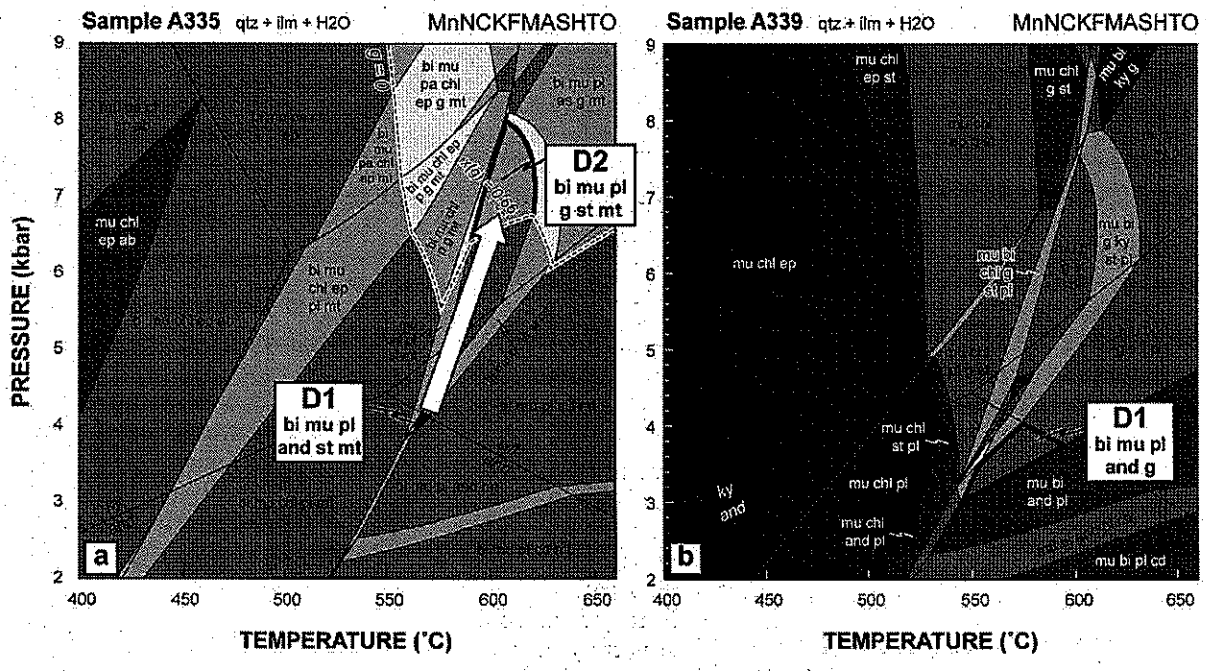

Figure 10. Pseudosections calculated for bulk rock compositions of samples A335 and A339.

growth of garnet at the expense of andalusite. As shown on the phase diagram, transitional equilibria from aluminosilicate to garnet stability require an increase in P (fig. 10*a*). A P-T estimate for the D_2 biotite, muscovite, plagioclase, garnet, staurolite, and magnetite assemblage is 0.64–0.8 GPa and 590°–620°C. Refinement of this estimate was achieved by calculating the compositional isopleth of the almandine content of garnet (Thermocalc variable $X_{alm} = Fe^{2+}/(Fe^{2+} = +Mg + Ca + Mn)$). Owing to the lack of compositional zoning in these garnets, it can be reasonably assumed that their compositions represent equilibrium conditions. If we use the measured almandine content of garnets in sample A335 (0.66; table A3), the calculated isopleth refines P-T to 0.67–0.7 GPa and 590°–610°C during D_2.

Sample A339. To verify the P-T conditions calculated for sample A335, a second phase diagram was calculated for a high-Al metapelite (fig. 10*b*; table A2). Sample A339 contains both D_1 and D_2 mineral assemblages, with S_1 defined by biotite and quartz and S_2 by biotite, quartz, graphite, ilmenite, and muscovite, wrapping around porphyroblasts of andalusite (chiastolite) replaced by prograde muscovite and retrograde, fine-grained white mica. Garnet occurs within andalusite and in the matrix where it occurs as atolls surrounded by retrograde chlorite, mixed-layer clay (chlorite-smectite?); S_2 is flattened against it, indicating that it grew pre-S_2. It lacks inclusion trails, preventing the timing of its growth relative to that of andalusite, to be determined. Post-D_2 chlorite porphyroblasts are common.

For the purposes of this study, it has been assumed that andalusite and garnet grew synchronously. On the basis of this assumption, P-T conditions that pertain to the stability of the D_1 biotite, muscovite, plagioclase, garnet, and andalusite assemblage can be restricted to 0.30–0.40 GPa and 540°–590°C (fig. 10*b*). Following this, a nonunique P-T path can be constrained by the breakdown of andalusite to white mica, alteration of garnet to chlorite plus biotite, and growth of post-D_2 chlorite.

Deformation-Metamorphic Framework for the Anakie Inlier

The temperatures during D_1 and D_2 events, as indicated by individual pseudosections, are slightly higher than those determined from the Ti-in-biotite geothermometer (table 1). The pseudosection for sample A335 shows an almost isothermal com-

pression pathway, with P increasing from approximately 0.4 GPa at T = 560°C to 0.64–0.79 GPa at T between 580° and 640°C. This change in P confirms that a substantial thickening of the crust took place during D_2. The b cell parameter data from D_2 white mica support this interpretation because they reflect upper intermediate-P conditions (Guidotti and Sassi 1986).

Petrographic observations indicate that D_3 was a low-temperature event because minerals such as quartz and white mica formed during D_2 show little recrystallization and well-developed intragranular strain features. Additionally, S_3 is a solution cleavage, and fine-grained white mica replacing porphyroblasts has a composition reflecting low-grade metamorphic conditions. The formation of chlorite porphyroblasts post-D_2 attests to low-T conditions existing late in the history of this area. Such features suggest that the rocks in the Anakie Inlier cooled during D_3 and thus followed a decompression-cooling pathway, eventually reaching low T and P (fig. 11).

These results argue against tectonic models involving compression followed by extension in the Anakie Inlier (Withnall et al. 1995; Wood and Lister 2004; Fergusson et al. 2005, 2007). According to these authors, D_2 was extensional on the basis of S_2 being a near-horizontal tectonic fabric. However, there is no additional evidence, such as the presence of a décollement zone and associated structures (e.g., mylonites, brittle fault zones), kinematic indicators showing downdip sense of movement, and changing mineral paragenesis, that would be related to exhumation. Further, the D_1 to D_2 P-T path defined in this study strongly contrasts with that recorded in modern-day core complexes (e.g., D'Entrecasteaux Islands [Baldwin et al. 1993], Dayman dome metamorphic core complex [Daczko et al. 2009]; fig. 11*B*). Alternatively, it has been suggested that the development of horizontal tectonic fabrics in some terrains could be related to extensional collapse of thickened crust (Sandiford 1989). Because the P-T pathway delineated for the rocks in this study supports concurrent burial during the development of the S_2 fabric, the application of this model to explain the tectonothermal history of the rocks in the study area is also questioned.

Although it may be argued that an extensional setting did not exist during D_2, the same cannot be said for D_1. This is because the geothermal gradient operating at the time was high according to the P (0.42–0.4 GPa) and T (570°–560°C) determined for the D_1 assemblage in sample A335 (~38°C/km). Furthermore, the possible growth of pre-D_1 chiastolite indicates that heat was fluxing into the terrain before penetrative deformation. This situation could readily take place if the crust was thinned during an earlier extensional phase and the high geothermal gradient was inherited by D_1. Alternatively, D_1 may have been an extensional event. No structural evidence, however, can be quoted to support the latter interpretation because kinematic indicators that may have formed during D_1 have been obliterated during D_2. On the basis of textural evidence, mineral associations, and geothermal gradients, an extensional setting before D_1 is favored.

On the basis of the P-T path we have delineated (fig. 11*A*), it is of interest that rocks located along the ancestral Delamerian margin record similar metamorphic histories. For example, high-grade rocks within and around the Early Cambrian Rathgen Gneiss (514 ± 5 Ma; Foden et al. 1999) in the

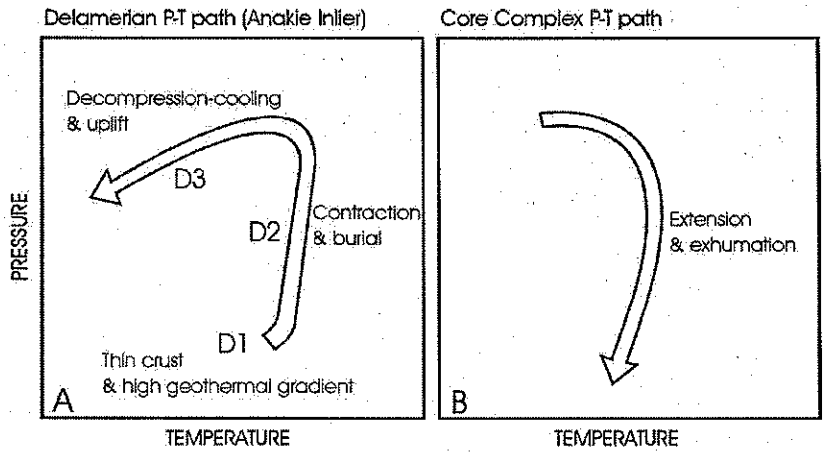

Figure 11. *A*, Delamerian pressure-temperature (P-T) path (Anakie Inlier). *B*, Core Complex P-T path.

eastern Mt. Lofty Ranges of the southern Adelaide Fold Belt record a subhorizontal gneissosity (Oliver and Zakowski 1995; Sandiford et al. 1995). This fabric formed during the Delamerian Orogeny (514–490 Ma; Foden et al. 2006) and is believed to have been produced during an earlier extensional event after the emplacement of the Rathgen Gneiss (Foden et al. 1999). Subsequently, a contractional event deformed this fabric (Sandiford et al. 1992, 1995; Oliver and Zakowski 1995).

Evidence supporting an extensional setting is the observation that pre-D_1 andalusite and staurolite occur in schists from the northern part of the Mt. Lofty Ranges (Fleming and Offler 1968). This implies that heat was fluxing into this terrain before penetrative deformation. Granitic magmas may have provided this heat because elevated *P-T* conditions are associated with the D_1 event (Sandiford et al. 1992, 1995). Clearly, if this model is to be applied to the Clermont region, further studies are required. These should involve the Gem Park Granite, an S-type foliated granite of possible Cambrian age that occurs southwest of Rubyvale (fig. 2). It intrudes the Bathampton Metamorphics, and smaller bodies have a foliation parallel to that in the metamorphics, suggesting that the two units were deformed together (Withnall et al. 1993, 1995). Dating of the granite, the muscovite and biotite-bearing foliation in it, and the metamorphic host would confirm or negate the model.

Metamorphic Zone Boundary Migration

Migration of the metamorphic zone boundaries appears to have occurred as deformation progressed, so that minerals stable during D_1 could not form because of a lowering of temperature during D_2. Evidence supporting this observation is recorded in the low-grade samples from the northeast of the study area that show the growth of biotite only during D_1 and lack of recrystallization of quartz and white mica deformed during D_2. This contrasts with the samples in the southwest, in which S_2 is defined by biotite. An additional observation supporting this apparent migration of metamorphic zone boundaries is that garnet porphyroblasts commonly grow post-D_1–early syn-D_2 but rarely post-D_2. Clearly, in the latter case, peak metamorphism was attained in most locations early syn-D_2. These features argue for a subsurface heat source that cools with time. What the source of the heat may be is not known. Subsurface magmatic bodies are an obvious choice because they would provide a heat flux only over a limited period. However, there is no geological or geophysical evidence yet to support this interpretation, as there is in other terrains (e.g., southern New England Fold Belt; Dirks et al. 1992). The Gem Park Granite southwest of Rubyvale is a possibility, but as pointed out previously, there is no reliable radiometric age for this pluton.

Implications for Local and Regional Tectonic Models

In the andalusite and staurolite-bearing schists, D_1 produced upright folds and axial planar foliation at conditions of 0.4 GPa and 560°C. This was followed by the development of a low-angle foliation and recumbent folds at $P = 0.64$–0.79 GPa and $T = 580°$–$640°C$ during D_2. The S_2 has subsequently been tilted westward at moderate to steep angles during D_3 and the mid-Carboniferous regional folding and faulting of the unconformably overlying Drummond Basin succession (Henderson et al. 1998). Crustal thickening took place during D_2 and is inconsistent with an extensional setting at this time, as suggested by Withnall et al. (1995), Fergusson et al. (2005), and Wood (2006). However, it is in agreement with models proposed by other authors for the deformation and metamorphism of the Late Proterozoic–Cambrian passive margin sediments in other locations along the eastern margin of Gondwana. For example, at Petrel Cove in the Mt. Lofty Ranges, South Australia, Alias et al. (2002) have shown that as deformation proceeds, metamorphic assemblages change as a result of an increase in *P* during cooling. This observation clearly indicates that crustal thickening has taken place. Tasmania records a similar history, with initial extension leading to rifting of a microcontinent and a developing arc, followed by contraction during arc accretion (Crawford and Berry 1992).

The timing of contraction in the Anakie Inlier provides an additional link to other orogens of Delamerian age. Contraction of the Anakie sequences can be constrained to the middle Cambrian on the basis of the depositional age for the Wynyard Metamorphics of ca. 510–500 Ma, the latter a metamorphic cooling age given by several whole-rock K-Ar ages (Withnall et al. 1996; Fergusson et al. 2001). Therefore, deformation and metamorphism of the Anakie Metamorphic Group are temporally related to the Delamerian Orogeny of southeastern Australia (Withnall et al. 1996; Foden et al. 2006). The timing of the Delamerian Orogeny has been reassessed and is considered to have been initiated at ca. 525 Ma or earlier (Turner et al. 2009), rather than at ca. 515 Ma, as thought previously (Foden et al. 2006). This older age is consistent with the timing of onset of significant convergent defor-

mation in the Ross Orogen (530–520 Ma; Foster et al. 2005). However, different ages of convergence along the Delamerian-Ross Orogeny have been previously reported in Antarctica (i.e., initiation at around 550 Ma; Goodge 1997).

The tectonic model we propose to explain the metamorphic signature in the rocks of the Anakie Inlier initially involved the rifting of the margin of Rodinia during the period 830–570 Ma (Cawood 2005). At some time within this period, the Anakie Inlier formed as a result of rifting of the margin and migration of a sliver of Rodinia to the east. Sedimentation continued periodically throughout this period at the passive margin and was terminated at ca. 500 Ma. We believe that mafic magmas that intruded the ca. 600-Ma Bathampton Metamorphics (Fergusson et al. 2009) and those underplating the passive margin sequences were responsible for raising the geothermal gradient, leading to the development of metamorphic assemblages pre-D_1. This high geothermal gradient was inherited by D_1 at the commencement of convergence, resulting in high-*T*/low-*P* metamorphism. The change from extension to convergence occurred over a short period, resulting in contraction and crustal thickening and greater tectonic burial of the rocks in the Anakie Inlier.

Conclusions

Metamorphism in the Anakie Metamorphic Group of the Anakie Inlier of central Queensland is characterized by low to moderate grades, with the development of chlorite, biotite, garnet, and andalusite ± staurolite zones in schistose metasedimentary rocks and nondefinitive chlorite-epidote ± actinolite assemblages in mafic schists. The structural history of these rocks reflects three main deformations, with D_1 associated with low-*P* metamorphism in the southwest of the study area (0.4 GPa, 560°C). During D_2, metamorphism changed to medium-*P* conditions, as shown by *P* values of 0.55 GPa in low-grade samples determined from *b* cell parameter data and of 0.64–0.79 GPa at 580°–640°C from pseudosections obtained from the staurolite-bearing rocks. During D_2, the isotherms retreated toward the southwest of the study area. Retrograde low-*P*/low-*T* metamorphism occurred during D_3.

These metamorphic conditions have implications for the tectonic history of the Anakie Metamorphic Group and the development of the Early Paleozoic active Gondwana margin in northeastern Australia. Previously, it has been considered that the largely flat-lying development of the S_2 foliation across the Anakie Inlier reflects extensional tectonics. The increasing metamorphic pressures from D_1 to D_2 indicate crustal thickening indicative of contractional deformation and inconsistent with crustal extension. D_2 is therefore related to a contractional phase of the Delamerian Orogeny in northeastern Australia at ca. 510–500 Ma (Withnall et al. 1996; Green et al. 1998; Fergusson et al. 2001). The context of D_1 is poorly constrained and has been considered contractional in the past but is associated with low-*P*/high-*T* metamorphism and could possibly reflect extension.

ACKNOWLEDGMENTS

We thank M. Rubenach for constructive criticism of the manuscript and Editor D. Rowley for editorial comments and changes. P. Johnson is gratefully acknowledged for drafting of figures 1–3 and J. Zhiyu for the remaining figures and preparation of thin sections. D. Phelan provided able assistance with the EDS analyses and SEM x-ray maps, J. Zobec the XRF analyses, and M. Davies the preparation of fused discs. T. Green acknowledges supervision and support in the field by P. Carr and B. Chenhall at the University of Wollongong. This research was funded from grants from the Australian Research Council, the University of Wollongong, and the University of Newcastle.

REFERENCES CITED

Alias, G.; Sandiford, M.; Hand, M.; and Worley, B. 2002. The *P-T* record of synchronous magmatism, metamorphism and deformation at Petrel Cove, southern Adelaide Fold Belt. J. Metamorph. Geol. 20:351–363.

Árkai, P.; Balogh, K.; and Frey, M. 1997. The effects of tectonic strain on crystallinity, apparent mean crystallite size and lattice strain of phyllosilicates in low-temperature metamorphic rocks: a case study from the Glarus overthrust, Switzerland. Schweiz. Mineral. Petrogr. Mitteil. 77:27–40.

Baldwin, S. L.; Lister, G. S.; Hill, E. J.; Foster, D. A.; and McDougall, I. 1993. Thermochronologic constraints on the tectonic evolution of the active core complexes, D'Entrecasteaux Islands, Papua New Guinea. Tectonics 12:611–628.

Cawood, P. A. 2005. Terra Australis Orogen: Rodinia breakup and development of the Pacific and Iapetus margins of Gondwana during the Neoproterozoic and Paleozoic. Earth-Sci. Rev. 69:249–279.

Coggon, R., and Holland, T. J. B. 2002. Mixing properties

of phengitic micas and revised garnet-phengite thermobarometers. J. Metamorph. Geol. 20:683–696.

Crawford, A. J., and Berry, R. F. 1992. Tectonic implications of Late Proterozoic–Early Palaeozoic igneous rock associations in western Tasmania. Tectonophysics 214:37–58.

Daczko, N. R.; Caffi, P.; Halpin, J. A.; and Mann, P. 2009. Exhumation of the Dayman dome metamorphic complex, eastern Papua New Guinea. J. Metamorph. Geol. 27:405–422.

Davis, B. K., and Henderson, R. A. 1998. Rift-phase extensional fabrics of the back-arc Drummond Basin. Basin Res. 8:371–381.

Deer, W. A.; Howie, R. A.; and Zussman, J. 1992. An introduction to rock-forming minerals. 2nd ed. Longman, Essex.

Dirks, P. H. G. M.; Hand, M.; Collins, W. J.; and Offler R. 1992. Structural-metamorphic evolution of the Tia Complex, New England Fold Belt: thermal overprint of an accretion-subduction complex in a compressional back-arc setting. J. Struct. Geol. 14:669–688.

Droop, G. T. R. 1987. A general equation for estimating Fe^{3+} concentrations in ferromagnesian silicates and oxides from microprobe analyses using stoichiometric criteria. Mineral. Mag. 51:431–435.

Fergusson, C. L.; Carr, P. F.; Fanning, C. M.; and Green T. J. 2001. Proterozoic-Cambrian detrital zircon and monazite ages from the Anakie Inlier, central Queensland: Grenville and Pacific-Gondwana signatures. Aust. J. Earth Sci. 48:857–866.

Fergusson, C. L.; Henderson, R. A.; Lewthwaite, K. J.; Phillips, D.; and Withnall, I. W. 2005. Structure of the Early Palaeozoic Cape River metamorphics, Tasmanides of north Queensland: evaluation of the roles of convergent and extensional tectonics. Aust. J. Earth Sci. 52:261–277.

Fergusson, C. L.; Henderson, R. A.; Withnall, I. W.; Fanning, C. M.; Phillips, D.; and Lewthwaite, K. J. 2007. Structural, metamorphic and geochronological constraints on alternating compression and extension in the Early Paleozoic Gondwanan Pacific margin, northeastern Australia. Tectonics 26:TC3008, doi:10.1029/2006TC001979.

Fergusson, C. L.; Offler, R.; and Green, T. J. 2009. Late Neoproterozoic passive margin of East Gondwana: geochemical constraints from the Anakie Inlier, central Queensland, Australia. Precambrian Res. 168: 301–312, doi:10.1016/j.precamres.2008.10.007.

Fleming, P. D., and Offler, R. 1968. Pre-tectonic metamorphic crystallisation in the Mt. Lofty Ranges, South Australia. Geol. Mag. 105:356–359.

Foden, J.; Elburg, M. A.; Dougherty-Page, J.; and Burtt, A. 2006. The timing and duration of the Delamerian orogeny: correlation with the Ross Orogen and implications for Gondwana assembly. J. Geol. 114:189–210.

Foden, J.; Sandiford, M.; Dougherty-Page, J.; and Williams, I. 1999. Geochemistry and geochronology of the Rathjen Gneiss: implications for the early tectonic evolution of the Delamerian Orogen. Aust. J. Earth Sci. 46:377–389.

Foster, D. A.; Gray, D. R.; and Spaggiari, C. 2005. Timing of subduction and exhumation along the Cambrian East Gondwana margin, and the formation of Paleozoic backarc basins. Geol. Soc. Am. Bull. 117:105–116.

Goodge, J. W. 1997. Latest Neoproterozoic basin inversion of the Beardmore Group, central Transantarctic Mountains, Antarctica. Tectonics 16:682–701.

Green, T. J.; Fergusson, C. L.; and Withnall, I. W. 1998. Refolding and strain in the Neoproterozoic–Early Palaeozoic Anakie Metamorphic Group, central Queensland. Aust. J. Earth Sci. 45:915–924.

Guggenheim, S.; Bain, D. C.; Bergaya, F.; Brigatti, M. F.; Drits, V. A.; Eberl, D. D.; Formoso, M. L. L.; et al. 2002. Report of the Association Internationale pour l'Etude des Argiles (AIPEA) Nomenclature Committee for 2001: order, disorder and crystallinity in phyllosilicates and the use of the Crystallinity Index. Clay Miner. 37:389–393.

Guidotti, C. V. 1984. Micas in metamorphic rocks. *In* Bailey, S. W., ed. Micas. Mineral. Soc. Am. Rev. Mineral. 13:357–467.

Guidotti, C. V., and Sassi, F. P. 1986. Classification and correlation of metamorphic facies series by means of muscovite b_0 data from low grade metapelites. Neues Jahrb. Mineral. Abh. 153:363–380.

Henderson, R. A.; Davis, B. K.; and Fanning, C. M. 1998. Stratigraphy, age relationships and tectonic setting of rift-phase infill in the Drummond Basin, central Queensland. Aust. J. Earth Sci. 45:579–595.

Henry, D. J.; Guidotti, C. V.; and Thomson, J. A. 2005. The Ti-saturation surface for low-to-medium pressure metapelitic biotites: implications for geothermometry and Ti-substitution mechanisms. Am. Mineral. 90: 316–328.

Hillier, S., and Velde, B. 1991. Octahedral occupancy and the chemical composition of diagenetic (low-temperature) chlorites. Clay Miner. 26:149–168.

Holland, T. J. B., and Powell, R. 1998. An internally consistent thermodynamic data set for phases of petrological interest. J. Metamorph. Geol. 16:309–343.

———. 2003. Activity-composition relations for phases in petrological calculations: an asymmetric multicomponent formulation. Contrib. Mineral. Petrol. 145:492–501.

Jiang, W.-T.; Peacor, D. R.; and Buseck, P. R. 1994. Chlorite geothermometry? contamination and apparent octahedral vacancies. Clays Clay Miner. 42:593–605.

Kisch, H. J. 1991. Illite crystallinity: recommendations on sample preparation, X-ray diffraction settings and interlaboratory standards. J. Metamorph. Geol. 9:665–670.

Kisch, H. J.; Árkai, P.; and Brime, C. 2004. On the calibration of the illite Kübler Index ("illite crystallinity"). Schweiz. Mineral. Mitt. 84:323–331.

Krumm, S., and Buggisch, W. 1991. Sample preparation effects on illite crystallinity measurements, grain size gradation and particle orientation. J. Metamorph. Geol. 9:671–678.

Kübler, B. 1968. Evaluation quantitative de métamorphisme par la cristallinité de l'illite. Cent. Rech. Pau Soc. Natl. Petrol. d'Aquit. Bull. 2:385–397.

Mahar, E. M.; Baker, J. M.; Powell, R.; Holland, T. J. B.; and Howell, N. 1997. The effect of Mn on mineral stability in metapelites. J. Metamorph. Geol. 15:223–238.

Murray, C. G. 1986. Metallogeny and tectonic development of the Tasman Fold Belt System in Queensland. Ore Geol. Rev. 1:315–400.

Oliver, N. H. S., and Zakowski, S. 1995. Timing and geometry of deformation, low pressure metamorphism and anatexis in the eastern Mt. Lofty ranges: the possible role of extension. Aust. J. Earth Sci. 42:501–507.

Parra, T.; Vidal, O.; and Agard, P. 2002. A thermodynamic model for Fe-Mg dioctahedral K white micas using data from phase-equilibrium experiments and natural politic assemblages. Contrib. Mineral. Petrol. 143: 706–732.

Powell, R., and Holland, T. Y. B. 1988. An internally consistent thermodynamic dataset with uncertainties and correlations: application, methods worked examples and computer program. J. Metamorph. Geol. 6:173–204.

Robinson, D. 1981. Metamorphic rocks of an intermediate facies juxtaposed at the Start boundary, southwest England. Geol. Mag. 118:297–301.

Sandiford, M. 1989. Horizontal structures in granulite terrains: a record of mountain building or mountain collapse? Geology 17:449–452.

Sandiford, M.; Foden, J. D.; Zhou, S.; and Turner, S. P. 1992. granite genesis and the mechanics of convergent orogenic belts with application to the southern Adelaide Fold Belt. Trans. R. Soc. Edinb. 83:83–93.

Sandiford, M.; Fraser, G.; Arnold, J.; Foden, J.; and Farrow, T. 1995. Some causes and consequences of high-temperature, low pressure metamorphism in the eastern Mt. Lofty Ranges, South Australia. Aust. J. Earth Sci. 42:233–240.

Sillanpää, J. 1986. Mineral chemistry study of progressive metamorphism in calcareous schists from Ankarvattnet, Swedish Caledonides. Lithos 19:141–152.

Turner, S.; Haines, P.; Foster, D.; Powell, R.; Sandiford, M.; and Offler, R. 2009. Did the Delamerian Orogeny start in the Neoproterozoic? J. Geol. 117:575–583.

Vernon, R. H.; Paterson, S. R.; and Foster, D. 1993. Growth and deformation of porphyroblasts in the Foothills terrane, central Sierra Nevada, California: negotiating a microstructural minefield. J. Metamorph. Geol. 11:203–222.

Warr, L. N., and Rice, A. H. N. 1994. Interlaboratory standardisation and calibration of clay mineral crystallinity and crystallite size data. J. Metamorph. Geol. 12:141–152.

White, R. W.; Pomroy, N. E.; and Powell, R. 2005. An in-situ metatexite-diatexite transition in upper amphibolite facies rocks from Broken Hill, Australia. J. Metamorph. Geol. 23:579–602.

White, R. W.; Powell, R.; Holland, T. J. B.; and Worley, B. A. 2000. The effect of TiO_2 and Fe_2O_3 on metapelitic assemblages at greenschist and amphibolite facies conditions: mineral equilibria calculations in the system K_2O-FeO-MgO-Al_2O_3-SiO_2-H_2O-TiO_2-Fe_2O_3. J. Metamorph. Geol. 18:497–511.

Withnall, I. W.; Blake, P. R.; Crouch, S. B. S.; Tenison Woods, K.; Hayward, M. A.; Lam, J. S.; Garrad, P.; and Rees, I. D. 1995. Geology of the southern part of the Anakie Inlier, central Queensland. Qld. Geol. 7, 245 p.

Withnall, I. W.; Blake, P. R.; Crouch, S. B. S.; Tenison Woods, K.; Hayward, M. A.; Rees, I. D.; and Hutton, L. J. 1993. Geological mapping of the Southern Anakie Inlier, Central Queensland. Prog. Rep. Qld. Gov. Min. J. 94:28–43.

Withnall, I. W.; Golding, S. D.; Rees, I. D.; and Dobos, S. K. 1996. K-Ar dating of the Anakie Metamorphic Group: evidence for an extension of the Delamerian Orogeny into central Queensland. Aust. J. Earth Sci. 43:567–572.

Wood, D., and Lister, G. 2004. Age and implications of core complex formation in Central East Queensland: 17th Australian Geological Convention, Hobart, February 2004. Geol. Soc. Aust. Abstr. 73:194.

Wood, D. G. 2006. Structural geology, tectonics, and gold mineralisation of the southern Anakie Inlier. Research School of Earth Sciences, Australian National University, Annual Report 2006.

Zane, A., and Weiss, Z. 1998. A procedure for classifying rock-forming chlorites based on microprobe data. Rend. Fis. Accad. Lincei 9:51–56.

Zhu, W., and Wei, C. 2007. Thermodynamic modelling of the phengite geobarometry. Sci. China 50:1033–1039.